Proceedings of the 11th ICPMG 2026
11th International Conference on Physical Modelling in Geotechnics
8-12 June 2026, Zurich, Switzerland

Field measurements using a model electrical vibrodriver for data-driven automation of the vibrodriving process

F. Williams-Riquer*[1], M. Cramer[1], M.A. Pick[2] , J. Grabe[1]

[1]*Institute of Geotechnical Engineering and Construction Management, Hamburg University of Technology, Hamburg, Germany, francisco.williams@tuhh.de**

[2]*Institute of Mechanics and Ocean Engineering, Hamburg University of Technology, Hamburg, Germany*

ABSTRACT: Vibrodriving is a widely applied technique for pile installation. It offers advantages over impact-driven methods, including reduced noise emissions, higher penetration rates, and reduced structural damage to piles. During vibrodriving, the driving parameters: primarily frequency and, in some cases, eccentric moment, are selected during installation by the operator according to prior soil investigations and empirical experience. Inappropriate selection may result in inefficient penetration, premature termination, or even mechanical failure of the vibrator. Therefore, increasing attention has been directed towards the development of automated strategies for the optimal selection of driving parameters. The complex interaction mechanisms governing the coupled vibrator-pile-soil system require comprehensive experimental investigations and data acquisition. However, full-scale field measurements and centrifuge experiments require considerable financial and logistical effort. To address these limitations, a model variable-moment vibrodriver was constructed and deployed for field measurements. This work presents the results of installing four open-ended tubular piles with a 30 mm diameter. The driving frequency (up to 30 Hz) and eccentric moment were manually adjusted to achieve penetration depths of approximately 80 cm. The results demonstrate the suitability of the developed device for further experimental investigations of the installation process and for generating high-quality datasets. Such datasets are intended to support data-driven automation and optimisation approaches, including the prediction of transmitted vibrations and the identification of cavitation and non-cavitation penetration modes. As an illustrative example, Dynamic Mode Decomposition is applied for equation-free modelling of vibrodriving-induced vibrations using geophone measurements.

1 INTRODUCTION

Installing profiles using vibrodriving is preferred due to its lower noise levels, reduced risk of pile damage, and faster penetration rates compared to impact driving. Nevertheless, its full acceptance in practice remains limited due to a lack of a comprehensive understanding of the nonlinear dynamics of the vibrator-pile-soil system (Massarsch et al., 2017). As a consequence, several industrial standards recommend completing the final driving phase with impact hammers to ensure the required bearing capacity (Rausche, 2002). The process presents conflicting objectives: rapid installation is desirable, yet vibrations transmitted to the surroundings must be minimised. Moreover, the bearing capacity of vibrodriven piles is not only lower than that of impact-driven piles but also dependent on the driving parameters, namely frequency and eccentric moment (Massarsch et al., 2017; Rausche, 2002).

Extensive research efforts have been undertaken to improve the understanding of vibrodriving, including numerous field measurement campaigns. A comprehensive overview of early large-scale tests is provided by Viking (2002), which includes the BBRI studies (Holeyman, 1993) and investigations conducted in Germany (Cudmani et al., 2000; Cudmani and Huber, 2000; Dierssen, 1994). More recent full-scale tests have demonstrated the influence of frequency and eccentric moment on penetration kinematics (Massarsch et al., 2021), while laboratory-scale experiments have examined the effects of driving frequency and crane-lowering speed on shaft and tip behaviour using industrial vibrators (Martinelli et al., 2025). Although field campaigns produce essential insights, they are expensive, logistically constrained, and often restricted to conditions acceptable within real construction projects. As a result, the available data typically lack the richness and variability required to capture the process's full nonlinear behaviour.

In vibrodriving, there are typically two modes of penetration: no-cavitation and cavitation. In the no-cavitation mode, the pile tip never separates from the soil. In the cavitation mode, the pile tip loses contact with the soil during the upward portion of the vibration cycle, and a gap (cavity) forms at the tip; contact is re-established only during the downward portion of the cycle. The penetration observed in cavitation mode mainly occurs because, during the unloading phase, the soil is stretched and weakened, and during downward motion, the pile drives into it (Cudmani and Manthey, 2019). Measurements identifying these penetration modes at laboratory scales and in field measurements have been reported by different authors (Cudmani and Huber, 2000; Cudmani and Manthey, 2019; Hoffmann et al., 2020).

Furthermore, the ground vibrations induced by vibro-driven pile installation are a major concern in practice, particularly in urban environments where vibration limits are imposed to protect nearby structures and sensitive infrastructure. Accurate characterization and modeling of these vibrations remain challenging due to complex, nonlinear, and nonsmooth interactions within the vibrator-pile-soil system.

Given the complexities present in the vibrodriving process, data-driven modelling and control techniques are increasingly attractive. Their success, however, depends critically on the availability of high-quality data covering a wide range of operating conditions. In practice, contractors are often reluctant to explore limiting or extreme scenarios due to safety, time, or performance constraints, which restrict the variability of the collected data. Data-driven strategies that do not rely on large datasets, such as the short-term predictive approach proposed by Williams-Riquer et al. (2024, 2025) and Abdennadher et al. (2025), offer a workaround for these limitations; however, they still require testing across a range of field conditions.

Laboratory studies offer greater control over boundary and loading conditions and have therefore played a central role in advancing modelling efforts. Model vibrators equipped with electrical motors and gearless synchronisation were introduced by Bingham et al. (2000) and Musgrave et al. (2000) to develop control strategies, while geotechnical studies investigated resistance mechanisms and driveability (Holeyman et al., 1999; Rodger and Littlejohn, 1980; Vogelsang et al., 2017). Nevertheless, laboratory testing alone is insufficient, especially when using geophones, which are difficult to use under laboratory conditions, thereby preventing a realistic assessment of vibration propagation.

This study presents an electrical miniature vibrodriver to address the need for an intermediate platform that combines laboratory-level reproducibility with field-level realism. Its design enables independent control of vibration frequency and eccentric moment by regulating the phase difference between the upper and lower eccentric mass pairs. The system was deployed during a field measurement campaign in medium- to dense-sand, where four tubular model piles were installed. Measurements were recorded from an accelerometer, a linear encoder, a force-torque sensor, and geophones placed in the surrounding soil. These measurements will be used as the first step towards a generation of richer datasets of field conditions that can be used for developing data-driven strategies.

The remainder of this publication is organised as follows. Section 2 presents the governing equations of motion of the model vibrodriver. Section 3 describes the model vibrodriver and its instrumentation. Section 4 outlines the field measurement programme. Section 5 presents results from recorded sensor data to demonstrate the platform's capability to capture key features of the vibrodriving process. Section 6 presents an example of a data-driven strategy that applies Dynamic Mode Decomposition to equation-free model the vibration measured by the geophones. Finally, Section 7 summarizes the main findings and discusses the implications for future data-driven modelling and automation of vibrodriving.

2 PRINCIPLES OF VIBRODRIVING

This section presents the equations of motion of the vibrodriving process, considering the model vibrodriver.

The vibratory action transmitted to the pile is commonly decomposed into two components: a dynamic component generated by the oscillating eccentric masses, and a static component arising from the downward-acting weight. In the case of the developed model vibrodriver, no static component is present, as all masses, including the vibrator housing and the pile, oscillate.

Accordingly, the vertical dynamics of the model vibrodriver during installation are expressed as

$$M\ddot{z} + c\dot{z} = F_{\mathrm{dyn}}\sin(\omega t + \alpha) - F_{\mathrm{soil}}(t, z, \omega), \tag{1}$$

where z (m), $\dot{z}$ (m/s), and $\ddot{z}$ (m/s^2) denote vertical displacement, velocity, and acceleration, respectively. The term c (Ns/m) represents the damping induced by friction within the guide rail along which the vibrator is constrained to move. The total oscillating mass is given by

$$M = m_{\mathrm{p}} + m_{\mathrm{h}} + m_{\mathrm{e}}, \tag{2}$$

where m_{p}, m_{h}, and m_{e} correspond to the masses of the pile, the vibrator housing, and the eccentric masses (kg).

The dynamic excitation force in Eq. (1) is given by

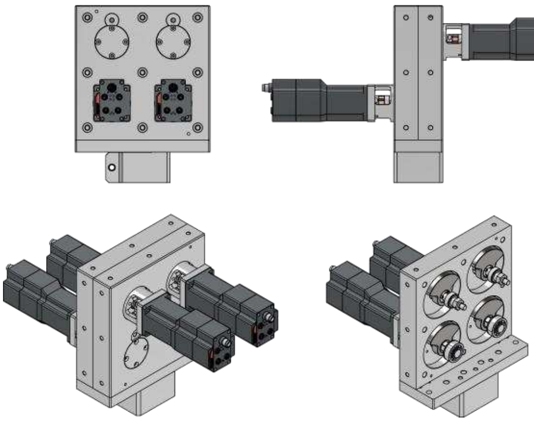

Figure 1.CAD model of the constructed vibrodriver.

$$F_{\text{dyn}} = m_{\text{e}} l \omega^2 \cos(\alpha/2) \qquad (3)$$

where l (m) is the eccentricity radius, ω (rad/s) is the angular rotation velocity, and α (rad) denotes the phase difference between the upper and lower pairs of eccentric masses. By adjusting α , the magnitude of the applied dynamic force can be systematically varied.

The term F_{soil}(N) represents soil resistance mobilised during vibratory penetration. There is literature presenting formulations attempting to describe this resistance as a function of penetration depth, excitation frequency, and penetration velocity (Dierssen, 1994; Holeyman and Whenham, 2017).

3 MODEL VIBRODRIVER

This section describes the model vibrodriver, including its mechanical components, integrated sensors, and control electronics.

A CAD rendering of the electrical gearless vibrodriver is shown in **Error! Reference source not found.**. The device consists of four identical eccentric masses, each directly driven by an individual servomotor. The main mechanical properties of the system are summarized in Table 1.

Table 1. Mechanical parameters of the model vibrodriver.

	Parameter	Value
m_{e}	Eccentric masses	0.772 kg
m_{p}	Pile mass	5.0 kg
m_{h}	Housing mass	19.23 kg
l	Equivalent radius	17 mm
d	Pile diameter	30 mm

The vibrodriver is mounted on a portable steel frame for transport and field deployment, as illustrated in Figure 2. A rope-and-pulley mechanism facilitates pile extraction after the experiments are concluded. For field operation, the electronic components are powered by a 36 V, 337 Wh lithium-ion battery pack. DC/DC converters supply the required voltages for the servomotors and the Beckhoff Programmable Logic Controller (PLC), which performs both control and data acquisition tasks.

The device is instrumented with several sensors to enable high-fidelity monitoring of the installation process. Each servomotor is equipped with a 17-bit absolute encoder, providing high-resolution measurements of shaft angular position and velocity and enabling precise phase control and amplitude modulation of the dynamic excitation force. Further instrumentation includes a triaxial integrated electronics piezoelectric (IEPE) accelerometer (KS943B10) mounted on the vibrodriver housing, a linear encoder (IMS Compact) attached to the guide rail to record vertical displacement, and an IEPE six-axis force-torque (9306A) sensor installed between the vibrator and the pile. Furthermore, four triaxial geophones (HL-6B) were arranged in a straight line from the vibrodriver, as shown in Figure 3, to measure particle velocity.

All sensor data are recorded and processed by the PLC with a 1 ms cycle time and a 1 kHz sampling rate.

Figure 2. Vibrodriver model used in field measurements.

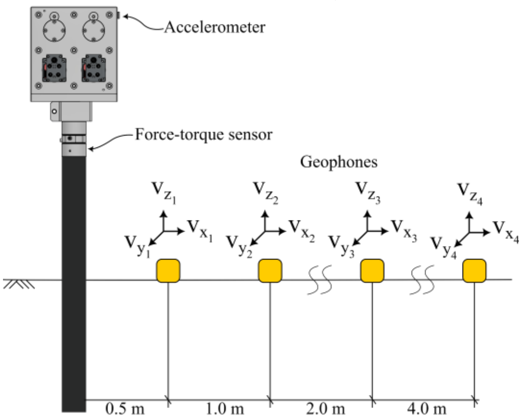

Figure 3. Positioning of geophones, accelerometer and force-torque sensor during pile installation.

4 SITE CHARACTERISATION AND MEASUREMENT PROGRAMME

This section presents the relevant parts of the field measurement campaign.

Before testing, 10 cm of a humus layer covered with roots was removed, and soil samples were collected to determine the grain-size distribution and loosest and densest densities. Undisturbed cylindrical samples were extracted to evaluate the in-situ density of the near-surface layer. Grain-size analyses of five samples revealed a consistent soil composition across the site, classified as fine sand containing up to 25% coarser sand and 8–11% fines (silt and clay). The sand was partially saturated, and the in-situ relative density in the near-surface layer ranged between $D_r = 0.83$ and $D_r = 0.93$. The corresponding soil properties are summarised in Table 2.

Table 2. Soil properties at the site.

	Parameter	Value
$\boldsymbol{D_{50}}$	Median grain size	0.144 mm
$\boldsymbol{C_{\mathrm{u}}}$	Coefficient of uniformity	2.38
$\boldsymbol{e_{\mathrm{max}}}$	Max. void ratio	1.162
$\boldsymbol{e_{\mathrm{min}}}$	Min. void ratio	0.346

Preliminary penetration tests indicated that the soil was too dense to allow installation of the test piles. Therefore, a 100 × 40 cm test area was prepared. The upper 80 cm was excavated. The soil in this zone was reconstructed in layers of 15 cm thickness and tamped after each layer to achieve a reduced density compared with the pre-excavation state. After preparation, the relative density ranged from $D_r = 0.66$ to $D_r = 0.74$.

The testing campaign consisted of installing four piles. Each pile was placed 20 cm from the boundaries of the prepared area and from adjacent piles. During installation, the excitation frequency (up to 30 Hz) and eccentric moment (0–100%) were varied to achieve maximum penetration. Three tests were performed at maximum amplitude. In these tests, the frequency was varied between 20 and 30 Hz using coarse (5 Hz) (denoted as P2) and fine (1 Hz) increments. In one test, the eccentric moment was increased stepwise at 20 Hz and the following section of 25 Hz and 30 Hz were driven with 100% amplitude (denoted as P1). Except for one pile, penetration depths exceeding 70 cm were reached.

5 RESULTS

This section presents the analysis of data collected during the installation of two of the four mentioned piles (P1 and P2) using the model vibrodriver.

Figure 4 (a) shows the vertical displacement of both piles, including the initial self-weight penetration and the subsequent displacement due to vibration. The vertical displacement shown in Figure 4 (a) for P1 and P2 is obtained by low-pass filtering the raw linear encoder displacement measurements to get the low-frequency component.

Figure 4 (b) shows the envelope of the oscillatory vertical force (F_{z}) during installation for P1 and P2. the measurement of F_z is related to the right-hand side of Eq. 1, which considers the dynamic force induced by the vibrodriver and the soil resistance. Figure 4 (b) shows an increase in the reaction force with depth. The force measurements are defined as positive when the load cell is in compression and negative when it is in tension. This convention, in contrast to Eq. 1, means that measurements of F_{z} will be increasingly positive as F_{soil} augments. The increase in the positive part of F_z during installation is thought to be related to an increase in soil density with depth and to densification in the vicinity of the pile's toe from induced vibrations. On the other hand, the negative measurements indicate resistance to upward movement during vibration, due to shaft resistance.

Figure 4 (c) shows the envelopes of the measured vertical components of particle velocity recorded by the four geophones, arranged as in Figure 3, for the installations of P1 and P2. These measurements capture the evolution of the vibration amplitude in the surrounding soil. As expected, geophones located closer to the pile register substantially higher vibration amplitudes than those farther away, indicating attenuation of vibratory energy with distance. A clear correlation is observed between the measured vertical force (F_{z}), shown in Figure 4 (b) and the geophone measurements, with peaks in the force envelope coinciding with higher particle velocities. These results confirm that the vibratory energy is effectively transmitted into the soil and that vibration intensity decays rapidly with distance from the pile shaft. Access to geophone data for field conditions enables the application of data-driven algorithms as shown in Section 6.

Figure 4 (d) shows the driving frequency during the installation of P1 and P2. The driving frequency is manually increased to achieve the desired penetration depth. The decision to increase driving frequency is made when penetration stagnates. The driving frequency is measured directly from the high-resolution absolute encoders in the servomotors.

Figure 4 (e) shows the amplitude of the eccentric moment, computed as

$$\text{Ecc. moment} = (1 - \alpha/\pi) \cdot 100\%,$$

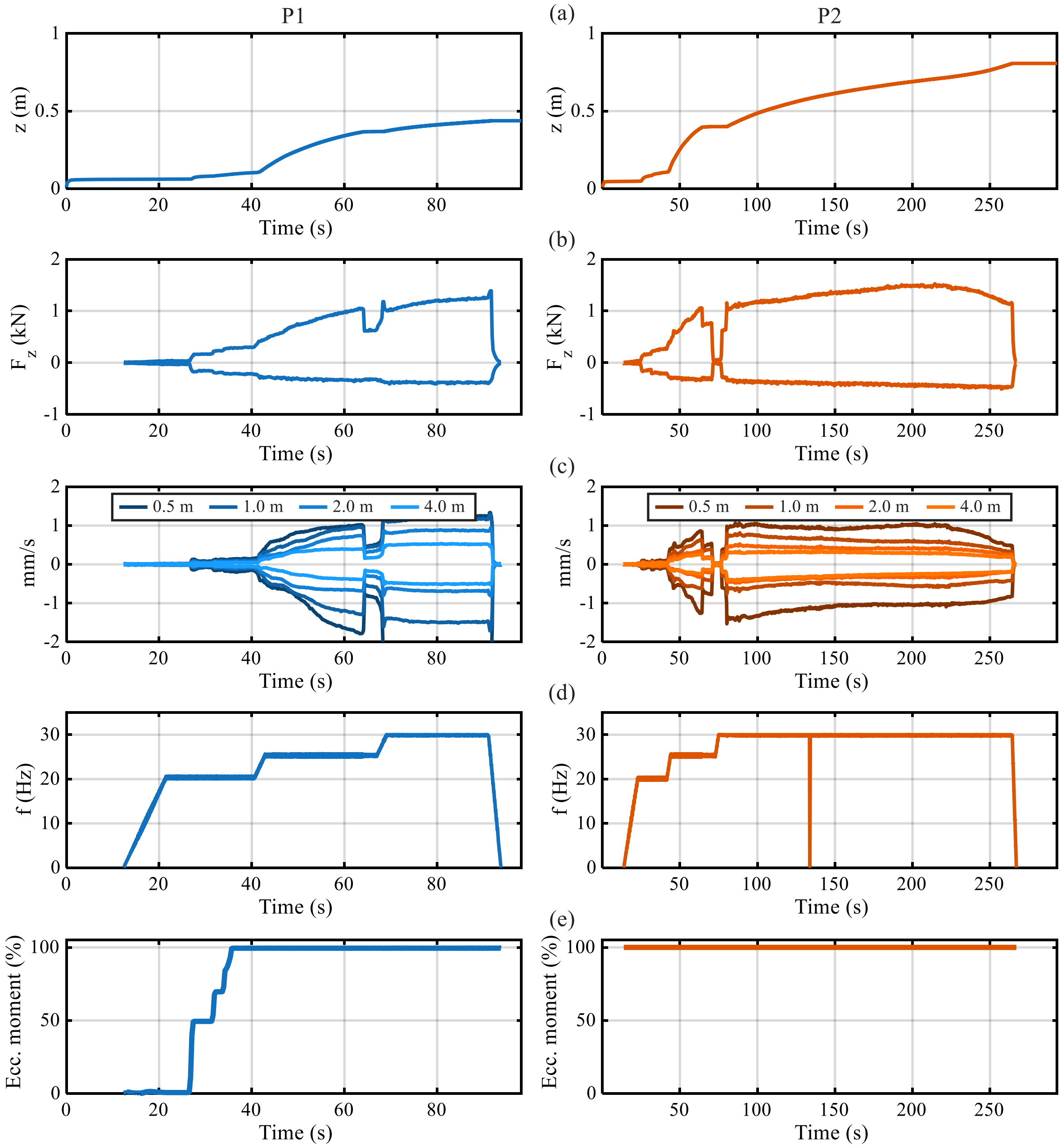

Figure 4. Penetration depth (a), envelope of the vertical force between vibrator and pile (b), vertical particle velocity from geophones (c), driving frequency (d), and ecc. moment (e) for the installation of P1 and P2.

for the installation of P1 and P2.

Notice that the force, frequency, vertical particle velocity, and amplitude signals are shown only for the periods during which the vibrator was active (i.e., non-zero rotational speed). In contrast, the penetration depth also includes the initial settlement under self-weight before the onset of vibrations. The differences in installation duration and penetration behaviour between P1 and P2 reflect variations in operating parameters and soil resistance encountered at each location.

Figures 5 and 6 show the force-displacement measurements with the corresponding acceleration for the time period. The two modes of penetration are identified from the measurement data: no-cavitation (Figure 5) and cavitation (Figure 6). Notice that the force-torque sensor is placed between the pile and the vibrator, essentially working as a very rigid spring that compresses and stretches with each vibrating cycle. Therefore, the measurements differ from direct force measurements at the pile's tip in that the negative values (corresponding to tension in the force-torque sensor) are considerably larger due to the influence of shaft resistance opposing upward movement.

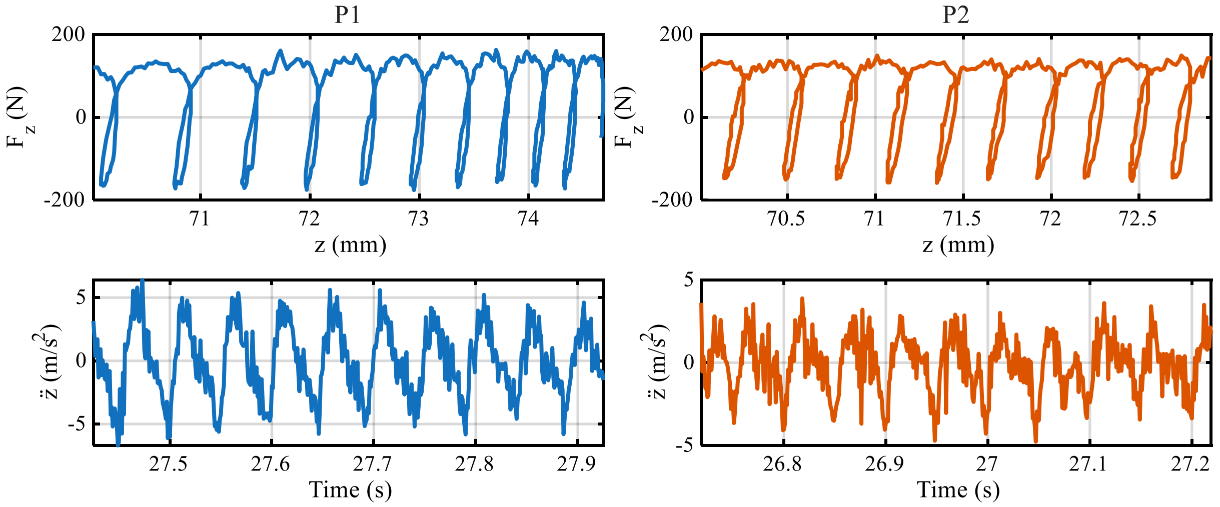

Figure 5. Vertical force vs. penetration depth (top) and vertical acceleration (bottom) showing no-cavitation penetration mode.

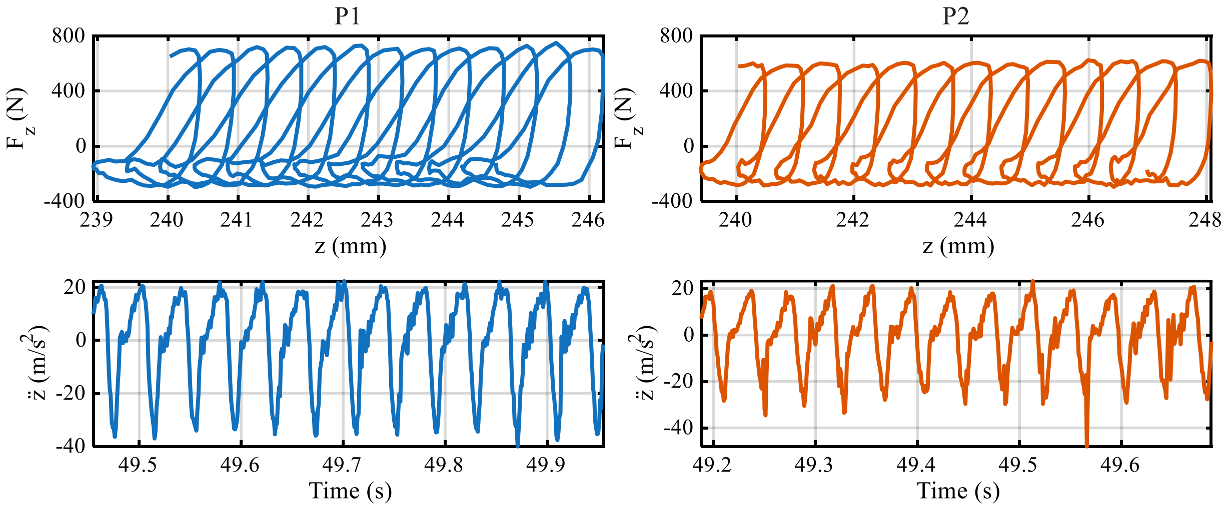

Figure 6. Vertical force vs. penetration depth (top) and vertical acceleration (bottom) showing cavitation penetration mode.

Access to reliable measurements enables identification of the penetration mode, thereby supporting the potential use of accelerometer data for automatic labelling of cavitational and non-cavitational behaviour, providing a foundation for future data-driven classification or control strategies.

6 DYNAMIC MODE DECOMPOSITION FOR VIBRODRIVING-INDUCED VIBRATIONS

This section presents preliminary results from applying Dynamic Mode Decomposition (DMD) with time-delay embedding for equation-free modeling of vibrations induced during vibrodriving. The objective is to demonstrate that the developed experimental platform generates data of sufficient quality and structure to enable meaningful modelling on using data-driven techniques.

To apply DMD, no prior knowledge of the governing physical equations is required. Instead, the system dynamics are inferred solely from the temporal evolution of the recorded signals. For a comprehensive explanation of DMD with time-delay coordinates, the reader is referred to (Williams-Riquer et al., 2024, 2025). DMD identifies dominant spatiotemporal patterns embedded in the measurement data. These patterns can be interpreted as coherent structures characterized by specific frequencies, growth or decay rates, and spatial distributions. In this way, complex vibration signals are decomposed into a small number of dynamically meaningful components. Figure 7 compares the 3D measurements (true) of the

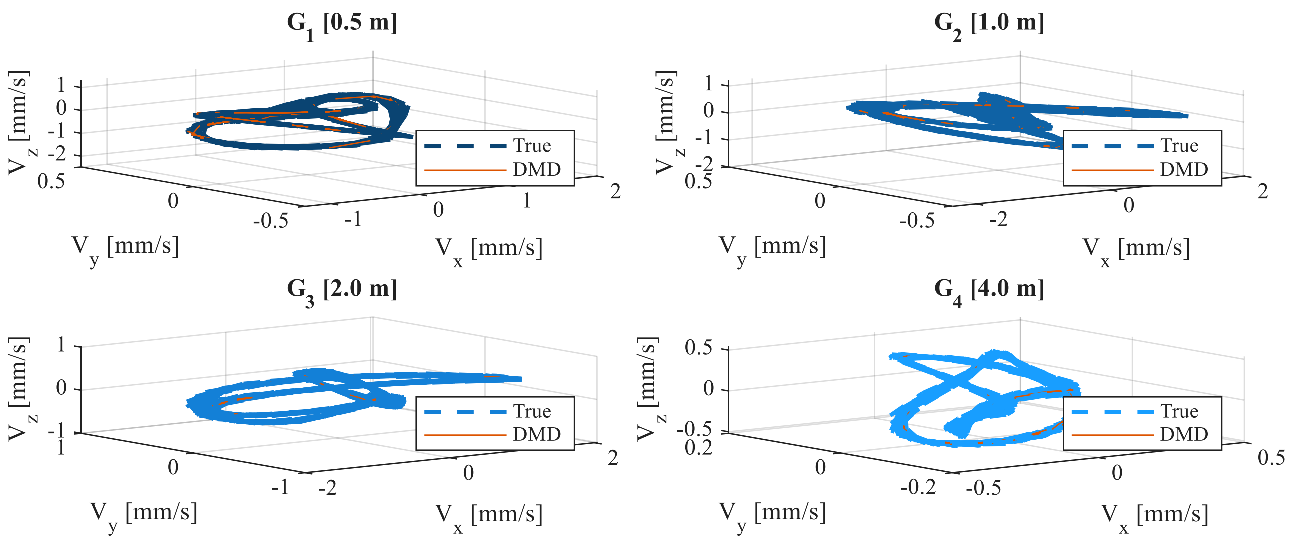

Figure 7. Comparison between measured (true) geophone data in the three axes and the DMD approximation for a 1.0-second time window for P1.

geophones over a 1.0-second window with the DMD approximation for the same time window for P1. The DMD can accurately recreate the measurements in time. Figure 8 shows the first four DMD modes corresponding to the first geophone at 0.5 m. DMD decomposes the measurements into a superposition of

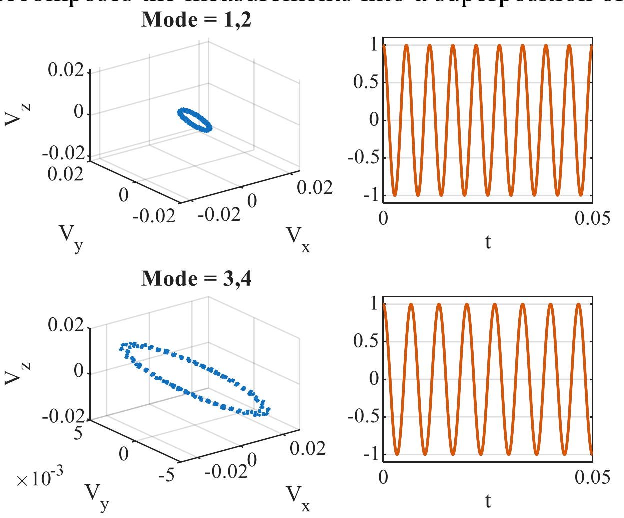

Figure 8. First four DMD modes for the closest geophone showing the spatial (left) and temporal (right) evolution.

linear spacial modes (left) modes evolving at different frequencies in time (right). A similar analysis can be carried out for all geophones.

7 CONCLUSIONS

This work presented a miniature electrical vibrodriver as a versatile experimental platform for investigating the vibrodriving process under realistic yet controllable conditions. To demonstrate its capabilities, four tubular piles were installed in medium- to dense sand, and high-resolution sensor data were acquired during installation. Manual control of excitation frequency and eccentric moment was performed, enabling systematic variation of the driving conditions throughout the installation process. Investigating automation strategies aims to develop automated methods for estimating optimal driving parameters to reduce manual adjustments.

The collected data demonstrate that the platform can capture key mechanisms governing vibrodriving, including cavitational and non-cavitational penetration regimes, as well as the propagation of vibrations through the surrounding ground. Deployment under field conditions reduced the influence of artificial boundary effects, allowing high-quality geophone measurements and a realistic assessment of vibration transmission. As an example of a data-driven strategy, DMD was applied to the collected geophone data for equation-free modeling and modal decomposition of the measured vibrations.

Overall, the results indicate the potential of the developed vibrodriver model as an effective intermediate platform between controlled laboratory experiments and full-scale field campaigns. The developed platform could be used to generate rich, high-quality datasets under controllable yet realistic conditions, making it well-suited for data-driven modelling, system identification, and the development of predictive and automation strategies for vibrodriving. Further field testing across a wider range of soil conditions, including looser and more homogeneous soils, is required to establish a benchmark for data collection and to improve the quality of particle velocity measurements.

Forthcoming work will focus on exploiting the collected data for predictive modelling and control of the vibrodriving process. In particular, vibrations transmitted to the surroundings can be predicted by recursively applying DMD to particle velocity measurements, enabling the optimal selection of driving parameters so that in-situ vibration limits are not exceeded. In addition, machine-learning approaches can be applied to labelled accelerometer data to automatically identify cavitation and non-cavitation penetration modes.

ACKNOWLEDGEMENTS

Funded by the Deutsche Forschungsgemeinschaft (DFG, German Research Foundation) – Project number: 471875774

REFERENCES

Abdennadher, M. A., F. Williams-Riquer, D. A. Dao, and J. Grabe (2025). "Data-driven modeling of structural dynamics: Improving measurement noise robustness with augmented dynamic mode decomposition." In: Proceedings of the 10th ECCOMAS Thematic Conference on Computational Methods in Structural Dynamics and Earthquake Engineering (COMPDYN 2025), Rhodes Island, Greece, 15–18 June 2025, edited by M. Papadrakakis and M. Fragiadakis.

Bingham, C. M., D. A. Stone, N. Schofield, D. Howe, and D. Peel (2000). "Amplitude and frequency control of a vibratory pile driver." IEEE Transactions on Industrial Electronics, 47 (3): 623–631. https://doi.org/10.1109/41.847903

Cudmani, R., and G. Huber (2000). "Development of a vibro-penetration test (VPT) for in-situ investigation of cohesionless soils." In: Vibratory pile driving and deep soil compaction - TRANSVIB2000., edited by V. & C. (eds.) Holeyman.

Cudmani, R., G. Huber, and G. Gudehus (2000). "A Mechanical Model for the Investigation of the vibro-drivability of piles in cohesionless soils." In: Proceedings: Vibratory pile driving and deep soil compaction - TRANSVIB2000., edited by V. & C. (eds.) Holeyman.

Cudmani, R., and S. Manthey (2019). "A novel vibro-penetration test (VPT) for the investigation of cohesionless soils in the field." Soil Dynamics and Earthquake Engineering, 126: 105760. https://doi.org/10.1016/j.soildyn.2019.105760

Dierssen, G. (1994). "Ein bodenmechanisches Modell zur Beschreibung des Vibrationsrammens in körnigen Böden." PhD Thesis, Universität Karlsruhe.

Hoffmann, B., J. Labenski, and C. Moormann (2020). "Effects of vibratory driving of monopiles on soil conditions and their cyclic lateral load bearing behavior." In: Proc., 4th Int. Symp. on Frontiers in Offshore Geotechnics. Rotterdam, Netherlands: CRC Press.

Holeyman, A. (1993). HIPERVIB1: An analytical model-based computer program to evaluate the penetration speed of vibratory driven sheet piles. Research Report. Belgian Building Research Institute (BBRI).

Holeyman, A., J. F. V. Berghe, and S. D. Cock (1999). "Toe resistance during pile vibratory penetration." In: Geotechnical Engineering for Transportation Infrastructure.

Holeyman, A., and V. Whenham (2017). "Critical Review of the Hypervib1 Model to Assess Pile Vibro-Drivability." Geotechnical and Geological Engineering, 35 (5): 1933–1951. https://doi.org/10.1007/s10706-017-0218-8

Martinelli, M., A. Tsetas, A. B. Fărăgău, A. Metrikine, and A. Tsouvalas (2025). "Soil resistance during vibratory pile installation: Experimental findings from lab-scale tests." Soil Dynamics and Earthquake Engineering, 199: 109692. https://doi.org/10.1016/j.soildyn.2025.109692

Massarsch, K. R., B. H. Fellenius, and A. Bodare (2017). "Fundamentals of the vibratory driving of piles and sheet piles." geotechnik, 40 (2): 126–141. https://doi.org/10.1002/gete.201600018

Massarsch, K. R., C. Wersäll, and B. H. Fellenius (2021). "Dynamic Ground Response during Vibratory Sheet Pile Driving." Journal of Geotechnical and Geoenvironmental Engineering, 147 (7): 04021043. https://doi.org/10.1061/(ASCE)GT.1943-5606.0002520

Musgrave, D. J., C. M. Bingham, D. A. Stone, and D. Howe (2000). "Modelling and multivariable control of a gearless, electrically actuated vibrator." IEE Proceedings - Electric Power Applications, 147 (5): 345. https://doi.org/10.1049/ip-epa:20000587

Rausche, F. (2002). "Modeling of vibrator driving." In: Proceedings of the international conference on vibratory pile driving and deep soil compaction, 21–32. Lisse, The Netherlands: Balkema.

Rodger, A. A., and G. S. Littlejohn (1980). "A study of vibratory driving in granular soils." Géotechnique, 30 (3): 269–293. https://doi.org/10.1680/geot.1980.30.3.269

Viking, K. (2002). "Vibro driveability: A filed study of vibratory driven sheet piles in non-cohesive soils." KTH.

Vogelsang, J., G. Huber, and T. Triantafyllidis (2017). "Experimental Investigation of Vibratory Pile Driving in Saturated Sand." Holistic Simulation of Geotechnical Installation Processes, Lecture Notes in Applied and Computational Mechanics, edited by T. Triantafyllidis, 101–123. Cham: Springer International Publishing.

Williams-Riquer, F., M. A. Abdennadher, A. Chmelnizkij, J. Grabe, and K. Smarsly (2025). "Modeling and Predicting Soil Vibrations During Vibrodriving Installation Using Noisy Data and Dynamic Mode Decomposition." In: Experimental Vibration Analysis for Civil Engineering Structures, Lecture Notes in Civil Engineering, edited by E. Caetano and Á. Cunha, 710–718. https://doi.org/10.1007/978-3-031-96110-6_69

Williams-Riquer, F., A. Chmelnizkij, D. Alkateeb, and J. Grabe (2024). "Prediction of induced soil vibration during pile vibrodriving using Dynamic Mode Decomposition (DMD)." Journal of Physics:

Conference Series, 2909 (1): 012002. https://doi.org/10.1088/1742-6596/2909/1/012002